Int. J. Nonlinear Anal. Appl. 16 (2025) 3, 323–329
ISSN: 2008-6822 (electronic)
http://dx.doi.org/10.22075/ijnaa.2024.33108.4927

Analytical investigation of the behavior of five-junction solar cell based on Ge layers and InAlGaAs and InAlGaP alloys

Shokoufeh Rasan[a], Zahra Alaie[a,b,*], Mehdi Riahinasab[a,b], S. Mohammadali Zanjani[a,b]

[a]Department of Electrical Engineering, Najafabad Branch, Islamic Azad University, Najafabad, Iran
[b]Smart Microgrid Research Center, Najafabad Branch, Islamic Azad University, Najafabad, Iran

(Communicated by Ehsan Kozegar)

Abstract

In recent years, we have witnessed significant advancements in the production of solar cells with a reduction in cost and an increase in their efficiency. One of the stages in creating advancements in new cells is evaluating their performance under different conditions using simulations before their fabrication. In this article, the structure of a multi-junction solar cell composed of Ge layers, InAlGaAs alloys, and InAlGaP alloys will be comprehensively examined. To achieve the highest efficiency, the lowest absorbing layer of the solar cell (Ge solar cell) will initially be optically simulated and then electrically simulated. After optimizing the Ge solar cell, the intermediate layers between the cells (tunnel junctions) and then the upper absorbing layers will be optimized in sequence. Optimization of solar cells in each absorbing layer refers to selecting the appropriate thickness, impurity density, and molar percentage of the layers to achieve the highest efficiency. According to simulation results, an efficiency of over 49% has been achieved for the 5-junction cell.

Keywords: five-junction solar cell, energy band gap, efficiency, short circuit current, open circuit voltage
2020 MSC: 70G10, 68Q06

1 Introduction

Multi-junction solar cells, due to absorbing the entire solar spectrum, exhibit significantly higher efficiency compared to single-junction solar cells [2]. So far, multi-junction solar cells have been investigated by several groups [2]. In reference [3], in 2006, a three-junction GaInP/GaInAs/Ge solar cell structure was studied. In this cell, an InxGa1-xAs intermediate absorbing layer with minimum molar percentage (x) was used for the best lattice constant matching with the germanium substrate. In article [9], the current-voltage characteristics of two-junction p++AlGaAs/n++GaAs and p++AlGaAs/GaAs solar cells have been simulated for use in the three-junction InGaP/(In)GaAs/Ge cell. Reference [4] reviews linear efficiency reduction methods and output power increase with temperature in photovoltaic solar cells. Reference [8] presents theoretical relationships governing the quantum efficiency, energy bandgap, current density, and fill factor of III-V multi-junction cells considering the temperature effect. In reference [6], AlGaInP with a 1.2eV bandgap, and AlGaAs with a 1.7eV bandgap, have been developed for implementing high-efficiency

*Corresponding author
Email addresses: shokofe.rasan@yahoo.com (Shokoufeh Rasan), alaie.zahra@yahoo.com (Zahra Alaie), m.riahinasab@pel.iaun.ac.ir (Mehdi Riahinasab), sma_zanjani@pel.iaun.ac.ir (S. Mohammadali Zanjani)

Received: January 2024 *Accepted:* April 2024

multi-junction solar cells. In reference [10], the highest efficiency for four-junction solar cells under concentrated light is reported to be approximately 38%. In reference [5], a 6-junction solar cell with 47.1% efficiency under 143-sun irradiation has been investigated.

2 Five-junction solar cell structure

Figure 1 depicts an overview of the proposed solar cell. In this figure, a 5-junction solar cell with the composition of InAlGaP/InGaP/InAlGaAs/InGaAs/Ge is illustrated. In each cell, window and emitter layers are positioned atop, followed by the pn or pin junction as the absorbing layer, and field and buffer layers beneath the absorbing layer. Additionally, tunnel junctions are embedded between each cell. The main objective of this article is to optimize the thickness and impurity density of different layers in each cell, from the lowest cell to the highest one. In addition to the layers of each cell, optimizing tunnel junctions also plays a crucial role in increasing the efficiency of the 5-junction solar cell. The (Al0.3Ga0.7)InP solar cell will be utilized as the top cell in the multi-junction solar cell.

Figure 2 illustrates the band structure of the 5-junction solar cell. In this figure, carriers must tunnel from one cell to another. The greater the slope of the conduction band curves and the greater the capacity, the more the movement of the carriers will be facilitated. Therefore, our goal is to achieve the best band structure and consequently the highest efficiency. The most important layers in multi-junction solar cells are the tunnel junctions, which are responsible for tunneling the carriers and directing them to the next cell. If tunnel junctions do not perform their role well, loss and recombination of carriers will occur.

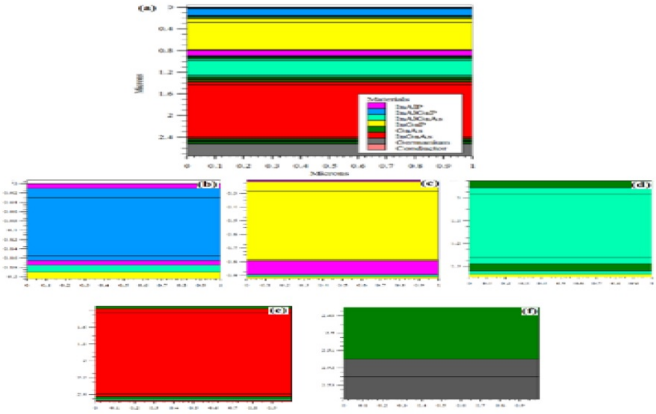

Figure 1: (a) An overview of the proposed five-junction solar cell in the article. (b) InAlGaP solar cell, (c) InGaP solar cell, (d) InAlGaAs solar cell, (e) InGaAs solar cell, (f) Ge solar cell.

Therefore, our goal is to achieve the best band structure and consequently the highest efficiency. The most important layers in multi-junction solar cells are tunnel junctions, which are responsible for tunneling carriers and guiding them to the next cell. If tunnel junctions fail to perform their role effectively, carrier recombination and loss will occur.

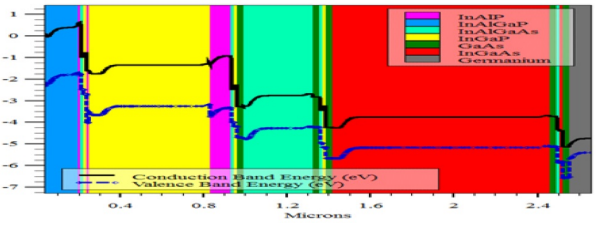

Figure 2: Five-junction solar cell strip structure

3 Governing equations for solar cell behavior

In numerical simulation of a solar cell, the "semiconductor equations" are solved for the specified solar cell structure. The semiconductor equations in one dimension consist of the Poisson equation and continuity equations. The Poisson

equation is related to the electrostatic potential ψ and the total charge density as follows [7]:

$$\frac{d^2\psi}{dx^2} = -\frac{q}{\varepsilon_s \varepsilon_0}[p(x) - n(x) + N_D^+ - N_A^- - \rho_{ds}(n,p)]. \tag{3.1}$$

The continuity equations, which relate the electron and hole currents to recombination and generation of electrons, are:

$$\frac{dJ_n}{dx} = G(x) - R(n,p) \tag{3.2}$$

$$\frac{dJ_p}{dx} = G(x) - R(n,p). \tag{3.3}$$

The Shockley-Queisser limit describes the effect of temperature on the bandgap and consequently the reduction of material efficiency. In this approximation, the dependence of material energy band gap on temperature is expressed by the following relationship [1]:

$$E_g(T) = E_g(300) - \frac{\alpha T^2}{T + \beta}. \tag{3.4}$$

4 Simulation results

Figure 3 shows the intensity of light emitted to the cell for a simulation time of 3000 femtoseconds. Based on this figure, the light reflection from the interface of different layers of the cell will increase the intensity of light irradiated to cell 3 compared to the rest of the cells, which should be considered in the electrical stimulation. This increase is caused by the back and forth-of light in this layer. In other words, the total absorption of the third cell is higher than the other cells. The remarkable thing about the third cell is that it is located exactly in the middle of the multi-junction cell, and the highest amount of light will travel back and forth and, as a result, the highest amount of absorption will be in this layer. This phenomenon also occurs for cell 4 at wavelengths of about 950 nm and 1150 nm. To consider this effect, we consider the increase or decrease of light intensity in each wavelength in the corresponding wavelength of the radiation spectrum to the cell in electrical simulation (Silvaco software).

By multiplying the intensity of light irradiated to each cell by the radiation spectrum of the sun, the spectrum irradiated to each cell will be obtained. Figure 4 shows the radiation spectrum for each cell. In this figure, the radiation spectrum of the solar cell (AM1.5) is multiplied by each of the spectra drawn in Figure 3, and as a result, the radiation spectrum of each cell is obtained. Based on this figure, the highest intensity of light will shine on the top cell, and as we move towards the lower cells, the intensity of the radiant light will decrease, especially in the lower wavelengths (due to light absorption in the upper cells).

Due to the reflection of light from the back surface of the solar cell, the intensity of the radiation spectrum to the third cell will be higher than the intensity of the radiation spectrum to the second cell at wavelengths higher than 800 nm.

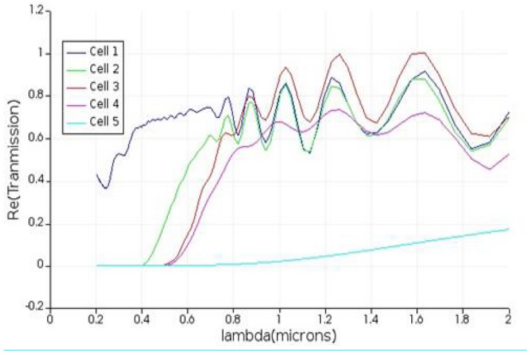

Figure 3: Radiant light intensity to each subcell

Figure 5 shows the electric field distribution at zero bias in the bottom Ge solar cell. In this figure, it shows the width of $x = 0.5\mu m$ from the top surface (distance from the top surface, zero nm) of the solar cell to the depth (distance from the top surface, $1.2\mu m$). Based on this figure, the two layers of the window and substrate at the beginning and

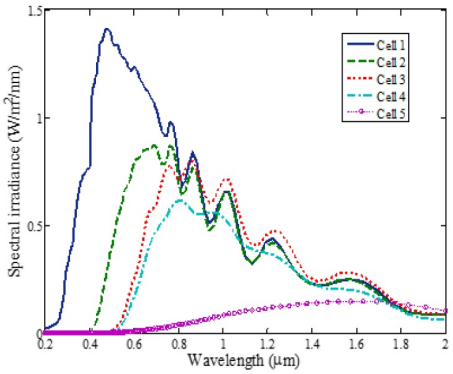

Figure 4: The spectral irradiance to each cell

end of the structure have a metallic state (n+ and p+) and the field in these two layers has a decreasing trend. At the border of the emitter and the base layer (at a depth of 10 nm) due to the formation of the p-n junction, the peak field intensity reaches 7.5e5V/cm. This peak of the field has the task of accelerating the electron-hole pairs produced outside the discharge region towards the discharge region and preventing their recombination.

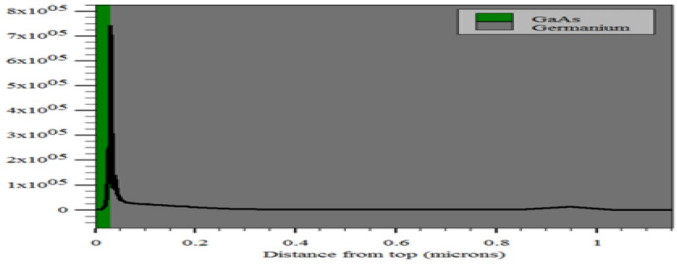

Figure 5: The distribution of the electric field at zero bias in the bottom Ge solar cell

Figure 6 shows the optical production and recombination rates in the depth of the underlying solar cell structure. In the recombination rate curve, the higher the impurity density, the higher the recombination. In the base layer, due to the lower impurity density, the recombination rate starts to decrease, so the lowest recombination rate of this structure can be seen in the base layer.

Another noteworthy point is the exponential decrease of absorption from the surface to the depth. From this reduction, we conclude that the closer the discharge area for this solar cell is to the surface, the higher the probability of production of electron-hole pairs and, as a result, the output optical current will be higher.

Figure 7 shows the current-voltage characteristic curve of the bottom solar cell under sunlight. From the current-voltage curve of the solar cell, it is possible to extract the evaluation parameters of the solar cell, such as short circuit current, open circuit voltage, maximum output power, efficiency and filling factor.

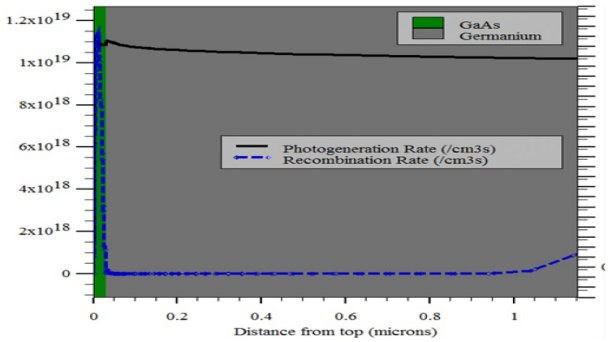

Figure 6: The rate of light generation in the bottom Ge solar cell structure

The slope of the current-voltage curve after switching on also shows the resistance of the connection. The turn-on

voltage of the diode (equivalent to the open circuit voltage of the solar cell) depends on the density of the junction impurity and the band gap of the absorbing semiconductor. The slope of the curve also depends on the resistance of the contact to the electrode. After absorbing light and producing electron-hole pairs, holes move towards the anode and electrons move towards the cathode, and a light current is created. In negative voltages, the photovoltaic or photodetective state is established. In fact, the radiation and absorption of sunlight will shift the current-voltage curve to negative voltages in the fourth quarter (positive voltage and negative current). Here the absolute magnitude of the current is plotted and the curve is displayed in the first quadrant. Also, a summary of the dependence of the functional parameters of the lower solar cell is presented in Table 1.

Figure 8 illustrates the current-voltage characteristic curve of 5 single-junction cells and thus the 5-junction solar cell. The summary of the dependence of the functional parameters of the solar cell is presented in Table 2.

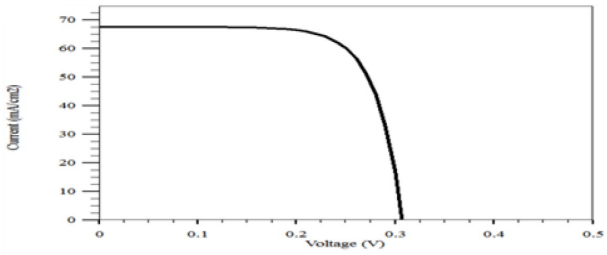

Figure 7: Illustrates the current-voltage characteristic curve of the fourth solar cell

Table 1: Summary of the dependence of performance parameters of the solar cell

$I_{SC}(mA/cm^2)$	$V_{OC}(V)$	$P_m(mW/cm^2)$	$FF(\%)$	$\eta(\%)$
67.5691	0.306848	15.0471	72.5741	10.8998

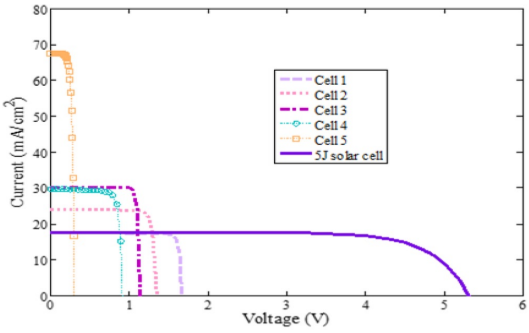

Figure 8: Current-voltage characteristic curve of a five-junction single-cell and a five-junction solar cell

Table 2: Summary of the dependence of performance parameters of the solar cell

$I_{SC}(mA/cm^2)$	$V_{OC}(V)$	$P_m(mW/cm^2)$	$FF(\%)$	$\eta(\%)$
17.576	5.383935	67.84316	71.24591	49.1442

Table 3: Summary of the dependence of performance parameters of the solar cell

	GaAs	**AlAs**	**AlGaAs**	**InP**	**GaP**	**InGaP**
me^*	$0.067 \times m0$	$0.71 \times m0$	$0.0919 \times m0$	$0.08 \times m0$	$0.17 \times m0$	$0.088 \times m0$
mh^*	$0.45 \times m0$	$0.804 \times m0$	$0.69 \times m0$	$0.5 \times m0$	$0.515 \times m0$	$0.7 \times m0$
ε	$13.1 \times \varepsilon 0$	$10.28 \times \varepsilon 0$	$12.31 \times \varepsilon 0$	$14.6 \times \varepsilon 0$	$11.11 \times \varepsilon 0$	$11.79 \times \varepsilon 0$

Figure 9 depicts the dependence of the energy gap of GaAs, AlAs, and AlGaAs as a function of temperature. According to the figure below, for all three materials, the energy gap decreases with increasing temperature with equal slope. With the decrease in the energy gap, we expect the maximum absorption wavelength to increase.

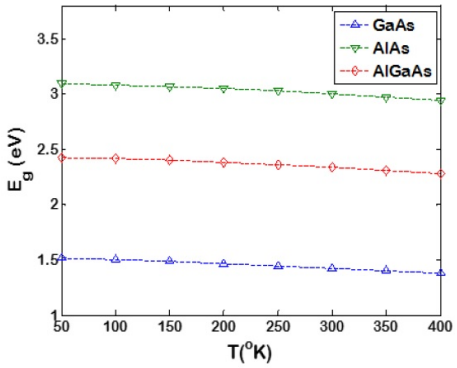

Figure 9: The temperature dependence of the energy gap for GaAs, AlAs, and AlGaAs

One of the important parameters of a semiconductor that depends on temperature is its electron affinity. In fact, changing the temperature according to the following relationship will change the electron seeking coefficients of GaAs and InGaP.

$$\chi(T) = \chi(300) - 0.5 \times (E_g(T) - E_g(300)) \tag{4.1}$$

Table 4: Dependence of the optical recombination coefficient of GaAs on temperature

Temperature (K)	**GaAs Radiative recombination coefficient (cm3/s)**
90	$1.8 \times 10 - 8$
185	$1.9 \times 10 - 9$
300	$7.2 \times 10 - 10$

Table 5: Dependence of Auger coefficient of GaAs on temperature

Temperature (K)	**GaAs Auger coefficient (cm6/s)**
300	10-30
500	10-29

Table 6: Dependence of optical recombination coefficient of InGaP on temperature

Temperature (K)	**InGaP Radiative recombination coefficient (cm3/s)**
300	$(1.0 \pm 0.3) \times 10 - 10$
150	$(4.0 \pm 1) \times 10 - 10$

Figure 10 shows the effect of temperature on the performance of the 5-link cell. According to this figure, with increasing temperature, VOC decreased drastically, but the short circuit current increased slightly.

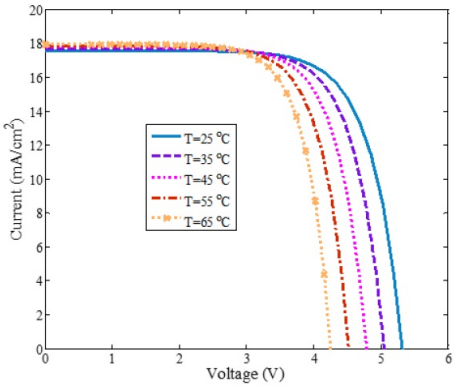

Figure 10: The effect of temperature on the performance of the five-junction cell

5 Conclusion

In this paper, the 5-junction solar cell was investigated optically and electrically. The structure of this multi-junction solar cell consisting of Ge layers, InAlGaAs alloys and InAlGaP alloys was comprehensively simulated for the first time. To achieve the highest efficiency, the lowest absorber layer of the solar cell (Ge solar cell) was optically simulated using Lumerical software, then we simulated electrically using Silvaco software. After optimizing the Ge solar cell, the intermediate layers between the cells (tunnel junctions) and then the higher absorber layers were optimized in order. The purpose of optimizing solar cells in each absorbent layer is to choose the appropriate thickness, impurity density and molar percentage of the layers in such a way that the highest efficiency is obtained. Based on the results of the simulation, an efficiency of more than 49% has been achieved for the 5-link cell.

References

[1] S. Adachi, *Band gaps and refractive indices of AlGaAsSb, GaInAsSb, and InPAsSb: Key properties for a variety of the 2-4 um optoelectronic device applications*, J. Appl. Phys. **61** (1987), no. 10, 4896–4876.

[2] A. Bates, *Novel optimization techniques for multijunction solar cell design using Silvaco ATLAS*, Master's Thesis, Naval Postgraduate School, 2003.

[3] F. Dimroth, *High-efficiency solar cells from III-V compound semiconductors*, Phys. Stat. Sol. (c) **3** (2006), 373–379.

[4] S. Dubey, J.N. Sarvaiya, and B. Seshadri, *Temperature dependent photovoltaic (PV) efficiency and its effect on PV production in the world*, Energy Proc. **33** (2013), 311–321.

[5] J.F. Geisz, R.M. France, K.L. Schulte, M.A. Steiner, A.G. Norman, H.L. Guthrey, M.R. Young, T. Song, and T. Moriarty, *Six-junction III–V solar cells with 47.1% conversion efficiency under 143 Suns concentration*, Nature Energy **5** (2020), no. 4, 326–335.

[6] J.F. Geisz, M.A. Steiner, N. Jain, K.L. Schulte, R.M. France, W.E. McMahon, E.E. Perl, K.A. Horowitz, and D.J. Friedman, *Pathway to 50% efficient inverted metamorphic concentrator solar cells*, AIP Conf. Proc. **1881** (2017), no. 1.

[7] S. Inc., *Atlas Manual*, Silvaco Inc., 2010.

[8] E.F. Fernández, A.J. García-Loureiro and G.P. Smestad, *Multijunction concentrator solar cells: Analysis and fundamentals*, P. Pérez-Higueras and E. Fernández, (eds) High concentrator photovoltaics, Green Energy and Technology, Springer, Cham, 2015.

[9] A.W. Walker, O. Thériault, M.M. Wilkins, J.F. Wheeldon and K. Hinzer, *Tunnel-junction-limited multijunction solar cell performance over concentration*, IEEE J. Select. Topics Quantum Electron. **19** (2013), no. 5, 1–8.

[10] X. Zhang, S. Huang, J. Liu, K. Lin, Y. Wang, and W. Yang, *Research on monolithic AlGaInP/AlGaInAs/GaInAs/Ge quadruple-junction solar cell for high efficiency lattice-matched tandem photovoltaic device*, Appl. Phys. Express **13** (2020), no. 7, 071002.